JOURNAL OF CATALYSIS 141, 438–452 (1993)

A Theoretical and Experimental Study of Catalytic Ignition in the Hydrogen–Oxygen Reaction on Platinum

M. FASSIHI,* V. P. ZHDANOV,*,† M. RINNEMO,* K.-E. KECK,* AND B. KASEMO*,[1]

*Department of Applied Physics, Chalmers University of Technology and University of Gothenburg, S-412 96 Göteborg, Sweden; and †Institute of Catalysis, Novosibirsk 630090, Russia

Received November 8, 1991; revised January 11, 1993

The catalytic ignition, i.e., the sudden transition from kinetic control to mass transport control, of nonflammable H_2/O_2 mixtures in N_2 at 1 atm, was in this work investigated experimentally and theoretically. Specifically the dependence of the ignition temperature (where the reaction self-accelerates due to the released chemical power) on the H_2/O_2 mixing ratio has been measured and simulated by model calculations. The latter take explicitly into account the surface kinetics of the reaction as well as mass and heat transport. The experimentally observed trend of increasing T_{ign} with increasing H_2/O_2 ratio can, via the simulations, be attributed to a combination of the hydrogen desorption kinetics and a weaker coverage dependence for H_2 sticking than for O_2 sticking on the surface. The numerical solution of the full model is compared with an approximate analytical expression for T_{ign}.

1. INTRODUCTION

Catalytic ignition (*1, 2*) is the phenomenon in exothermic surface-catalyzed reactions where the temperature and reaction rate self-accelerate due to heating of the substrate via the released chemical power. More precisely the ignition temperature, T_{ign}, is defined (*1*) as the temperature where the derivative, with respect to temperature, of the released chemical power in the reaction becomes larger than the corresponding derivative of the total power loss [due to cooling by the gas, radiation, and heat conduction (*1, 2*)]. Prior to ignition, the rate of the reaction is primarily controlled by the reaction kinetics and the mass and temperature gradients are weak. After ignition, in steady state, the reaction is primarily mass transport controlled and mass and temperature gradients may therefore be strong.

The phenomenon has both practical and scientific interest. For example, catalytic ignition (light-off) in catalytic car exhaust converters is a prerequisite for their proper function; prior to ignition the catalytic converter does not clean the exhaust gases. From a scientific point of view, catalytic ignition is an interesting transient phenomenon and a central ingredient in certain kinds of catalytic reaction oscillations. The ignition condition can also, in principle, be used to extract kinetic information.

The literature on catalytic ignition is extensive (*2–10*). As a rule, the surface kinetics are not treated explicitly in the theoretical models, but rather represented by assumed or empirical dependencies of the reaction rate on reactant concentrations in the gas phase, close to the catalyst surface. An explicit treatment requires a kinetic model, including a description of how surface coverages depend on gas-phase concentrations close to the surface, on desorption from and reaction on the surface etc. An approach of this type, including a treatment of the coupled surface kinetics mass and heat transport problem, is taken here for the H_2–O_2 reaction on Pt. The treatment is partly based on earlier work in our laboratory (*7*). A similar approach has been used

[1] To whom correspondence should be addressed.

0021-9517/93 $5.00

for CO oxidation on Pt by Harold and Garske (*8–10*).

We present new experimental data and a theoretical model that describes the dependence of T_{ign} on the H_2/O_2 ratio in nonflammable H_2/O_2 mixtures in N_2 at 1 atm. The main objective was to measure and understand, via the theoretical model, the dependence of T_{ign} on the H_2/O_2 ratio. In our treatment, we use a different and, as we argue below, a more realistic model than recently employed by Russberg (*7a*) to analyze early experimental data (*11–13*) from our laboratory. [In Ref. (*7a*) the coverage dependencies of oxygen and hydrogen adsorption were identical, and the known (*14, 15*) coverage dependence of the rate constant for H_2 desorption was not included.] The kinetic model used here has been described in a recent publication (16), where the model is shown to give excellent agreement with experimentally measured kinetics for OH and H_2O production on Pt in H_2/O_2 mixtures at pressures ≤100 mTorr and temperatures 1000–1300 K. Thus the kinetic model was originally designed for experimental conditions other than those in this work. The fact that it produces good agreement also with the present data lends additional support for the model.

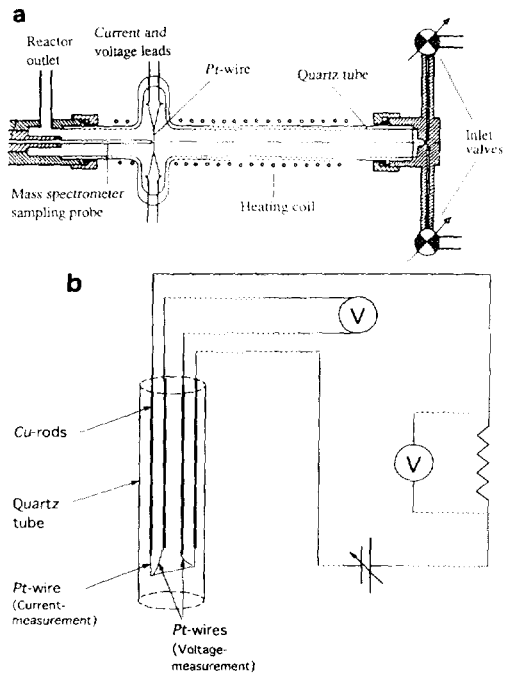

FIG. 1. (a) The early ignition temperature measurements were performed in a system with on-line mass spectrometry to follow H_2 and O_2 consumption and H_2O production, as described in Refs. (*11, 18*). (b) The measurements presented here were made in a modified version of the reaction cell in order to optimize the ignition temperature measurements, without perturbation from the mass spectrometer sampling device. In this case the gas mixture is injected into the cell, while the temperature of the catalyst can be derived from the resistivity of Pt. The temperature is externally controlled by a constant current generator.

2. EXPERIMENTAL SYSTEM AND PROCEDURE

Details of the experiment have been described before (*11*). In short, it consists of flowing a gas mixture of typically <4% H_2 and <20% O_2 in N_2, at a constant total pressure of 1 atm, over a Pt wire of 0.127 mm diameter and 17 mm length (Fig. 1). The reactant pressure $p_{H_2} + p_{O_2}$ was kept constant at 45 Torr. The nominal purity of the platinum wire, obtained from Material Research Corporation, was 99.995%. It is known that platinum contains Si. It has been shown, however, that this impurity may be removed by proper high-temperature treatment in H_2/O_2 mixtures (*13*). This method has been improved further by cycles of extensive heating in oxygen (~600 K, 20 min), followed by immersion in hydrofluoric acid (pro analysi, 40%). The effect of this treatment is manifested in slower passivation (increase in ignition temperature; see Keck and Kasemo (*13*)] of the Pt wire in the reaction mixture. It is therefore likely that the purity of the wire after these treatments actually was higher than the number quoted above.

A typical gas-flow velocity was 0.9 cm/s. In this velocity range the measured T_{ign} is quite insensitive to variation in flow velocity. The wire is mounted diametrically in a cylindrical quartz tube (ϕ = 19 mm, length 22 cm), in a four-point probe arrangement to allow simultaneous resistive heating and

temperature measurement of the Pt wire via its temperature-dependent resistivity. Consumption of H_2 and O_2 can be measured mass spectrometrically by sampling gas very close (~0.1 mm) to the catalyst (Fig. 1a). Most of the present measurements were, however, made without mass spectrometric control (Fig. 1b). Reasonable surface purity control is achieved via the value of T_{ign} at a fixed H_2/O_2 mixture, as calibrated by Auger electron spectroscopy (*13*). When the cleaning procedure developed in (*13*) was followed, and short time allowed between cleaning and ignition, reproducible data with low scatter were obtained. More specifically this procedure was as follows.

The catalyst was cleaned from adsorbed impurities for 2 min in a reactant mixture with $\alpha = 0.15$ at 1350 K in a flow of 550 cm^3/min (3.2 cm/s). [Here and below α is defined as $\alpha \equiv p_{H_2}/(p_{H_2} + p_{O_2})$, where p_{H_2} and p_{O_2} are the partial pressures of H_2 and O_2, respectively.] Then, the reactor was cooled by a flow of N_2 through the reactor, and externally by forced air convection, for 2 min. The desired reactant mixture was thereafter introduced and the system allowed to stabilize for 2 min. The temperature of the wire was then increased by successively increasing the current in small steps. The steps were adjusted such that the time needed to reach the ignition temperature was always approximately 2 min for all probed α-values. Well below ignition the temperature stabilized at a constant value after 5–10 s (i.e., steady state was established after each step). After the ignition trace had been recorded (Fig. 2), the next measurement was started with a new cleaning procedure. The sensitivity of the T_{ign} measurements to the duration of the experiment was significant but not too large. If, for example, the wire was held for 13 min at 385 K in an $\alpha = 0.67$ reactant mixture, prior to the ignition run, the ignition temperature increased ~10 K above the mean value obtained with the standard procedure, due to contamination.

The high-temperature treatments of the Pt sample in H_2/O_2 mixtures result in extensive recrystallization and facetting. As discussed in (*17*), this can give rise to large crystalline grains, probably with (111) surfaces, which can influence the absolute rate of conversion and to some extent sticking coefficients. However, it will not influence the main point of concern here, namely the variation of T_{ign} with α and its kinetic origin.

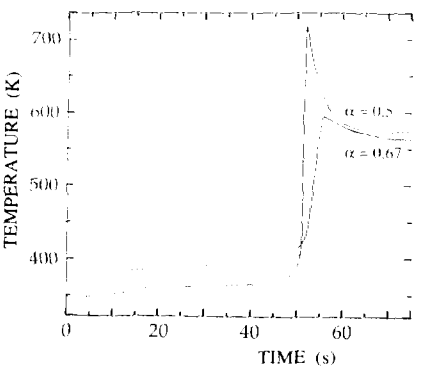

FIG. 2. Measured catalyst temperature as a function of time for $\alpha = 0.5$ and 0.67, respectively. In both cases the total pressure of the gas mixture is 760 Torr and $p_{H_2} + p_{O_2} = 45$ Torr. The behavior of the T vs time trace is explained in the text.

3. EXPERIMENTAL RESULTS

Figure 2 shows two recorded "ignition traces" (for $\alpha = 0.5$ and $\alpha = 0.67$, respectively), after two consequent small stepwise increases in the external heating current. After the last stepwise increase in the current, the temperature first increases slowly due to the thermal inertia of the system and then rapidly. The experimental ignition temperature is here taken as the point where the temperature started to self-accelerate in the T vs time trace (this empirical definition of T_{ign} is equivalent to the Frank–Kamenetskii criterion). A more detailed discussion of the definition of the ignition temperature will be given in a forthcoming publication.

The overshoots in the T vs t curves, just after ignition, are due to temporarily larger concentrations of reactants just outside the catalyst surface, because the steady-state

reactant gradients in the mass-controlled regime have not yet been established. Ignition temperatures were measured, as in Fig. 2, for a large number of α-values. The results are compiled in Fig. 7 and discussed in Section 5. The magnitude of the error bars in Fig. 7 derives mainly from uncertainties in α. The vertical error bars are comparable with the diameter of the filled circles.

The main focus of our analysis in the next paragraphs is the observed monotonic rise in T_{ign} with increasing α (Fig. 7). This increase is contrary to what one might intuitively have expected, based on an assumption of simple, competitive adsorption/desorption kinetics for H_2 and O_2, since the activation barrier for hydrogen desorption is much lower than that for oxygen desorption.

For large α-values the ignition becomes less and less distinct, and for $\alpha > 0.75$ an ignition step cannot be distinguished. For α-values <0.1, no experimental points are presented. The reason is a rapid drop in ignition temperature, with poor reproducibility and ignition already at or below room temperature. Possible reasons for both these results are discussed later.

4. THEORETICAL MODEL

The modeling proceeds along the following lines. Since it is possible to establish a steady state at any temperature below T_{ign}, we can approximate the system by steady-state solutions both for the kinetics and for the mass and heat transport, to simulate T_{ign} vs α. For the kinetics we employ a simplified version of a recently developed model (*16*), of the Langmuir–Hinshelwood type, including the essential known features of the hydrogen–oxygen reaction kinetics on polycrystalline platinum. For mass and heat transport we derive analytical expressions using the cylindrical symmetry around the wire catalyst and taking into account a finite gas-flow velocity. The influence of mass transport is weak, prior to and at ignition, due to the fairly low conversion rate of reactants to H_2O in this regime, which permits us to use a simplified treatment of the mass and heat transport. For the latter, a linear dependence of the catalyst temperature is assumed, which is supported by measurements with nonreactive N_2/H_2 and N_2/O_2 mixtures.

4.1. *Kinetics*

The kinetics of the hydrogen–oxygen reaction has been studied by many groups [see the review (*19*) and references in recent publications (*16–18, 20–26*)]. It is generally accepted that the dominant reaction is of the Langmuir–Hinshelwood type and occurs via one of the following steps for water formation:

$$H^a + OH^a \rightarrow H_2O \qquad (1)$$

$$OH^a + OH^a \rightarrow H_2O + O^a, \qquad (2)$$

where the superscript a refers to adsorbed particles. In the full model (*16*), hydrogen and oxygen adsorbs dissociatively and competitively. H and O react to form OH. OH reacts along (1) and/or (2) to form H_2O, which desorbs. For the present purpose it is sufficient to employ a simplified version of the full model. The simplifications are outlined below and are detailed in (*16*). The reaction is known to be quite fast at room temperature and above, due to fairly low activation barriers [chemisorbed oxygen and hydrogen react on Pt with measurable rate even at temperatures as low as 120 K (*22, 23, 27*)]. This has several important consequences (*16*): (i) It means that the reaction kinetics can be described in the steady-state (SS) approximation at least up to, but even during ignition; (ii) the steady-state reaction rate is in fact independent of which of the routes (1) or (2) that dominates; and (iii) at the temperatures and reactant pressures of interest the oxygen and hydroxyl desorption rates are negligible and the adsorption rates of oxygen and hydrogen are small in comparison with the rate constants corresponding to OH and H_2O formation. The surface is therefore (prior to ignition) covered predominantly by hydrogen (i.e., $\Theta_O \ll \Theta_H \approx \Theta$) in the hydrogen excess regime, and by

oxygen (i.e., $\Theta_H \ll \Theta_O \approx \Theta$) at sufficiently large oxygen excess (Θ_O, Θ_H, and Θ are the hydrogen, oxygen, and total coverages, respectively). In the former case, the hydrogen desorption compensates the hydrogen excess and we have

$$2S_{O_2}(\Theta)F_{O_2} + k^d_{H_2}\Theta^2 = S_{H_2}(\Theta)F_{H_2}, \quad (3)$$

where $S_{O_2}(\Theta)$ and $S_{H_2}(\Theta)$ are the coverage-dependent sticking coefficients, F_{O_2} and F_{H_2} are the surface impingement rates, which are proportional to the reactant pressures near the platinum wire, and $k^d_{H_2}$ is the desorption rate constant for hydrogen. Equation (3) expresses that all oxygen molecules that stick on the surface react with hydrogen to form water and that all stuck hydrogen molecules either react to water or desorb.

In the oxygen excess case, the hydrogen desorption rate is to a first approximation negligible due to low coverage and rapid reaction with oxygen. Oxygen desorption is negligible due to the large activation barrier for desorption. The reaction kinetics in this regime are thus described by

$$2S_{O_2}(\Theta)F_{O_2} = S_{H_2}(\Theta)F_{H_2}. \quad (4)$$

(Note that the coverage dependence of S_{H_2} must be weaker than that of S_{O_2}, otherwise we obtain the trivial solution of Eq. (4) that the oxygen coverage is equal to one in the oxygen excess regime.)

The rate of water production, $r^f_{H_2O}$, is in both cases equal to twice the rate of oxygen adsorption

$$r^f_{H_2O} = 2S_{O_2}(\Theta)F_{O_2}. \quad (5)$$

By changing the reaction conditions [e.g., changing the relative hydrogen pressure in the reactant mixture, $\alpha = p_{H_2}/(p_{H_2} + p_{O_2})$], one can force the system from one excess regime to the other. At very high temperatures, $T \approx 1000$ K, when the hydrogen coverage is low, the transition from dominance of hydrogen (oxygen) to oxygen (hydrogen) on the surface occurs at $2S_{O_2}(0)F_{O_2} = S_{H_2}(0)F_{H_2}$, which can be used to obtain the zero coverage sticking coefficients for H_2 and O_2 (*16*). In the present case, however, the situation is somewhat more complex (see below).

To calculate the kinetics, the following functions are used to describe the adsorption/desorption processes:

$$S_{O_2}(\Theta) = S_{O_2}(0)(1 - \Theta)^x \quad (6)$$

$$S_{H_2}(\Theta) = S_{H_2}(0)(1 - \Theta)^y \quad (7)$$

$$k^d_{H_2} = \nu\exp[-(E^0_d - A\Theta^z)/T], \quad (8)$$

where $S_{O_2}(0) = 0.02$ and $S_{H_2}(0) = 0.05$ are the sticking coefficients at low coverages (*16*), $\nu = 10^{13}$ s^{-1} the preexponential factor for hydrogen desorption, and $E^0_d = 19$ kcal/mol the desorption activation energy for hydrogen at low coverages (*14, 15, 28*) (here and below, Boltzmann's constant is set to unity). The available data on the parameter A and exponents x, y, and z are as follows:

(i) Thermal desorption (*14*) and adsorption isotherms (*15*) for hydrogen on Pt(111) can be reasonably described (*28*) by employing $A = 7$ kcal/mol and $z = 1$.

(ii) The coverage dependence of the hydrogen sticking coefficient on Pt(111) is rather strong ($y \geq 2$) if the surface is covered by hydrogen (*14, 19*) and weak [$y = 1$ (*19*) or $y = 0$ (*21, 29*)] if the surface is covered by oxygen. On the other hand, the hydrogen sticking coefficient for polycrystalline platinum is fairly weakly dependent on coverage ($y < 1$) even if the surface is covered by hydrogen (*30*).

(iii) The coverage dependence of the oxygen sticking coefficient can be described by Eq. (6) with $x = 2$ if the surface is covered by oxygen (*31, 32*). Data for the surface covered by hydrogen are not available.

(iv) We do not need to consider the weak T-dependencies of the sticking coefficients (*14, 20, 31, 33, 34*).

Our simulations show that the Pt surface before and during ignition is covered by hydrogen (if α is not too small). After ignition, the surface is covered by oxygen up to α around 0.43. For larger α it is predominantly hydrogen covered even after ignition (see

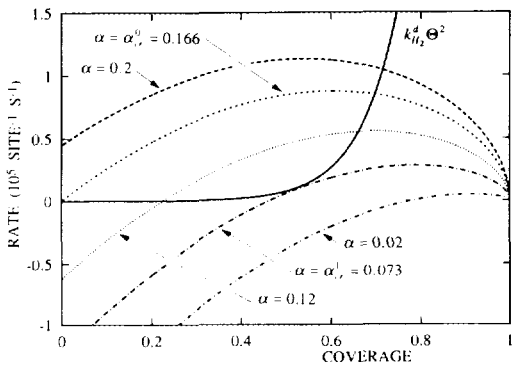

FIG. 3. Graphic solution of Eq. (3) for $x = 2$, $y = 0.5$, $z = 1$, $A = 7$ kcal/mol, $p_{H_2} + p_{O_2} = 45$ Torr, and $T = 400$ K. The curve labeled $k^d_{H_2}\Theta^2$ (solid line) shows the hydrogen desorption rate, as a function of coverage. The other curves show the coverage dependence of the difference between the hydrogen adsorption rate and the doubled oxygen adsorption rate, i.e., $S_{H_2}(\Theta)F_{H_2} - 2S_{O_2}(\Theta)F_{O_2}$. At $\alpha > \alpha^0_{cr}$, Eq. (3) has a single solution (α^0_{cr} is defined by the condition $S_{H_2}(0)F_{H_2} = 2S_{O_2}(0)F_{O_2}$). At $\alpha^1_{cr} < \alpha < \alpha^0_{cr}$, Eq. (3) has two solutions. At $\alpha = \alpha^1_{cr}$, Eq. (3) again has only one solution. Finally, at $\alpha < \alpha^1_{cr}$, Eq. (3) has no solution. In the latter range (and also at $\alpha^1_{cr} < \alpha < \alpha^0_{cr}$) Eq. (4) applies. Its solutions are simply the intersection of the adsorption differences curves with the abscissa. The curves correspond to $\alpha = 0.2$, $\alpha = \alpha^0_{cr} = 0.166$, $\alpha = 0.12$, $\alpha = \alpha^1_{cr} = 0.073$, and $\alpha = 0.02$, respectively.

below). In the postignition regime the reaction rate is limited by reactant diffusion to the surface. Thus, the dependence of the sticking coefficients on the oxygen coverage is of minor importance for the present treatment, and we assume that this dependence is the same as when the surface is covered by hydrogen. In addition, on the basis of the available data (*21, 29–32*), we assume that the coverage dependence of the oxygen sticking coefficient is stronger than that for hydrogen ($y < x \approx 2$–3).

If $x > y$, Eq. (3), with expressions (6)–(8), has a unique solution at $\alpha > \alpha^0_{cr}$ (see the graphic solution in Fig. 3), where with our choice of initial sticking coefficients, $\alpha^0_{cr} = 0.17$. Note that α^0_{cr} corresponds to the specific condition $2S_{O_2}(0)F_{O_2} = S_{H_2}(0)F_{H_2}$. For this condition one might conclude that the surface is uncovered. In reality this will not be the case, however, since if the coverage were very close to zero, but finite, the asymmetry in sticking coefficients would cause the hydrogen coverage to increase, until the advantage in the sticking coefficient for hydrogen, compared to oxygen, would be compensated by hydrogen desorption.

When $\alpha^1_{cr} < \alpha < \alpha^0_{cr}$, Eq. (3) has two solutions, Θ_1 and Θ_2 ($\Theta_1 > \Theta_2$). Stability analysis of these solutions, based on the linearized time-dependent equation for the hydrogen coverage, shows that the first solution is stable and the second is unstable (and again the physical reason is the asymmetry in the sticking coefficients). Finally, when $\alpha < \alpha^1_{cr}$, Eq. (3) has no solution. Thus, the point $\alpha = \alpha^1_{cr}$ corresponds to a transition from Eq. (3) to Eq. (4); i.e., at this point there is a discontinuous change in coverage and reaction rate (Fig. 4).

For $\alpha < \alpha^1_{cr}$, we thus have solutions corresponding to Eq. (4) (in Fig. 3., they are the points where the curves corresponding to $2S_{O_2}(\Theta)F_{O_2} - S_{H_2}(\Theta)F_{H_2}$ cross the abscissa). These solutions are stable and describe the surface covered by oxygen. Thus, for $\alpha < \alpha^1_{cr}$, the surface will always be covered predominantly by oxygen. The solutions of Eq. (4) for the interval $\alpha^1_{cr} < \alpha < \alpha^0_{cr}$ are also stable within the mean-field approximation and with the assumption of fast surface reaction steps.

Figure 4 illustrates these points further. For $\alpha > \alpha^0_{cr}$ and $\alpha < \alpha^1_{cr}$ there are unique solutions to Eqs. (3) and (4) that correspond to a predominantly hydrogen- and oxygen-covered surface, respectively. In the range $\alpha^1_{cr} < \alpha < \alpha^0_{cr}$ there are two stable SS solutions corresponding to hydrogen- or oxygen-covered surfaces. Which solution applies depends on how the SS condition has been approached. For example, if it were approached from large α-values, the surface would be covered by hydrogen, and vice versa. At α^1_{cr} (and α^0_{cr}), discontinuous transitions can occur from a hydrogen (oxygen) to an oxygen (hydrogen)-covered surface. This generates a hysteresis in surface cover-

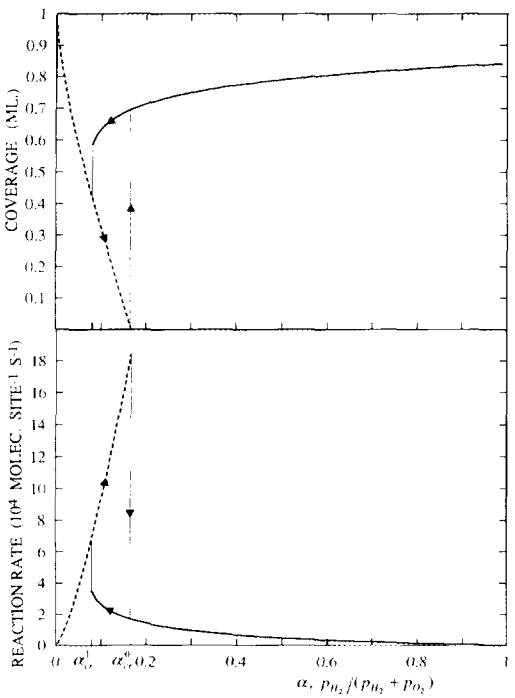

FIG. 4. Coverage and reaction rate as a function of the relative hydrogen pressure. At $\alpha > \alpha_{cr}^{0}$, the surface is covered by hydrogen. At $\alpha < \alpha_{cr}^{l}$, the surface is covered by oxygen. In the intermediate range, $\alpha_{cr}^{l} < \alpha < \alpha_{cr}^{0}$ the surface may be predominantly covered by either oxygen or hydrogen, depending on how the SS condition was established. The results were obtained with the same values of the various parameters as in Fig. 3. Pointers show a clockwise and anti-clockwise hysteresis in the reaction rate and coverage, respectively.

age and reaction rate, if a cycle is generated from $\alpha > \alpha_{cr}^{0}$ to $\alpha < \alpha_{cr}^{l}$ and back. In other words, the model predicts "kinetic phase transitions." Similar phenomena are known from kinetic models describing CO oxidation on Pt-group metals (*35*, *36*). In this case, the hysteresis serves as a cornerstone of kinetic oscillations. In this context it is relevant to note the experimental difficulty in obtaining reproducible T_{ign} values for $\alpha \leq 0.1$ (see Section 3). This may actually be connected with the kinetic complexity for $\alpha_{cr}^{l} < \alpha < \alpha_{cr}^{0}$ and motivates further experiments in this interesting regime.

The value of α_{cr}^{l} depends on temperature. With increasing temperature, the rate of hydrogen desorption increases (i.e., $k_{H_2}^{d}$ increases), and accordingly $\alpha_{cr}^{l} \rightarrow \alpha_{cr}^{0}$, while in the limit $k_{H_2}^{d} \rightarrow 0$ we have $\alpha_{cr}^{l} \rightarrow 0$.

Concluding the discussion of the bistable region (i.e., $\alpha_{cr}^{l} < \alpha < \alpha_{cr}^{0}$), it is important to note that the solutions to Eqs. (3) and (4), describing the surface covered by hydrogen and oxygen (Fig. 4), are stable if we employ the mean-field kinetic equations and do not take into account fluctuations, e.g., of adsorbed species on the surface due to surface diffusion. Including the latter process results in the possibility of forming "trigger" or chemical waves [see e.g. (*37–39*)]. In effect, accounting for surface diffusion, it is possible to introduce a new parameter α_{cr}^{*} ($\alpha_{cr}^{l} < \alpha_{cr}^{*} < \alpha_{cr}^{0}$). In the bistable region, the solution corresponding to the surface covered by oxygen is absolutely stable at $\alpha < \alpha_{cr}^{*}$ and metastable at $\alpha_{cr}^{*} < \alpha < \alpha_{cr}^{0}$. The solution describing the surface covered by hydrogen is metastable at $\alpha_{cr}^{l} < \alpha < \alpha_{cr}^{*}$ and absolutely stable at $\alpha > \alpha_{cr}^{*}$. A more detailed analysis of the effect of surface diffusion on stability of the solutions to Eqs. (3) and (4) shows that in our case $\alpha_{cr}^{*} \approx (\alpha_{cr}^{0} + \alpha_{cr}^{l})/2$ (*40*).

Equations (3) and (4) above are valid provided that the H_2–O_2 reaction is fast; i.e., the rate constants corresponding to OH and H_2O formation and H_2O desorption are large compared to the rates of hydrogen and oxygen adsorption [then the requirement for our analysis of Eqs. (3) and (4), i.e., $\Theta \approx \Theta_H$ and $\Theta \approx \Theta_0$, respectively, will be fulfilled; see also the discussion in Ref. (*16*)]. Physically these equations describe the two regimes of the reaction when (i) adsorbed hydrogen blocks oxygen adsorption [Eq. (3)] and (ii) adsorbed oxygen blocks hydrogen adsorption [Eq. (4)]. When the condition above of sufficiently large rate constants is not fulfilled, e.g., at sufficiently low temperature, the OH and H_2O formation steps and coverages must be treated explicitly. Our estimations show that at temperatures above 300 K the reaction can be considered as "fast" if the activation energies for OH

and H_2O formation are lower than 7 kcal/mol.

4.2. Heat and Mass Transport

The influence of mass transport on the ignition originates from the depletion of reactants near the catalyst surface when the reaction becomes sufficiently fast. Since the stoichiometry of the reaction is $H_2 + \frac{1}{2}O_2 \rightarrow H_2O$ and since the diffusion rates of H_2 and O_2 are different and finite, the reaction will inevitably reduce the absolute and change the relative concentrations near the catalyst. Thus, as soon as gradients are established, the local α-value just outside the surface will be different than for the unreacted gas. The effect is particularly important after ignition. (All α-values below refer to the α-value of the unreacted gas.)

If sufficiently large, the rate of temperature increase up to the ignition temperature will also affect T_{ign}. This effect is, however, negligible in the present case because the rate of temperature increase in the experiment was very small. We can therefore use the steady-state approximation to describe the heat and mass transport processes (the limitations of this approach are discussed in Section 5.2). The SS analysis is of particular importance in understanding the ignition process because the ignition criterion is then well known (*1*).

To solve the diffusion equations at a finite gas-flow velocity, w, we may separate a cylindrical region near the platinum wire. The radius of the region, R, should be chosen such that diffusion in this region dominates over gas flow. The opposite condition should be fulfilled outside the region. Using characteristic time scales for diffusion and gas flow, respectively, which can be estimated by $\tau_{dif} \approx R^2/D$ and $\tau_{fl} \approx R/w$, where D is the diffusion coefficient, we obtain the optimal value of R by requiring $\tau_{dif} = \tau_{fl}$, i.e., $R = D/w$. Then the diffusion equation at $r \leq$ R can be solved in the SS approximation, assuming that the reactant concentrations at $r \geq R$ are the same as those for the unreacted gas mixture.

Note that the value of R is dependent on the reactant gas. For hydrogen ($D_{H_2} = 0.63$ cm^2/s), we have $R_{H_2} = 1.6$ cm, and $\tau_{dif} = 4$ s. The corresponding values for oxygen ($D_{O_2} = 0.18$ cm^2/s) are $R_{O_2} = 0.4$ cm, and $\tau_{dif} = 1$ s. A similar analysis for the heat transfer (gas heat conductivity, $\lambda = 0.024$ W/m · K) from the wire to the gas yields $R_{ht} = 0.4$ cm and $\tau_{ht} = 1$ s.

The SS hydrogen concentration gradient (the number of gas-phase molecules per unit volume), obtained by solving the two-dimensional diffusion equation, is

$$n_{H_2}(r) = \begin{cases} n^0_{H_2} & \text{at } r > R_{H_2} \\ n^0_{H_2} + (n^s_{H_2} - n^0_{H_2}) \dfrac{\ln(R_{H_2}/r)}{\ln(R_{H_2}/r_s)} & \text{at } r_s < r < R_{H_2}, \end{cases}$$

where $n^s_{H_2}$ and $n^0_{H_2}$ are the gas-phase concentrations at and far from the surface, respectively, and r_s is the wire radius. The oxygen concentration gradient is equivalently obtained.

The two-dimensional thermal conductivity equation yields

$$T(r) = \begin{cases} T_0 & \text{at } r > R_{ht} \\ T_0 + (T_s - T_0) \dfrac{\ln(R_{ht}/r)}{\ln(R_{ht}/r_s)} & \text{at } r_s < r < R_{ht}. \end{cases}$$

By employing the expression above for the hydrogen concentration gradient, we can represent the diffusion flow f_{H_2} and impingement rate F_{H_2} (per site) of this reactant as

$$f_{H_2} = \frac{\sigma D_{H_2}(n^0_{H_2} - n^s_{H_2})}{r_s \ln(R_{H_2}/r_s)} \tag{9}$$

and

$$F_{H_2} = \sigma \sqrt{\frac{T}{2\pi m_{H_2}}}\, n^s_{H_2}, \tag{10}$$

where $\sigma \approx 4$ Å^2 is the site area, and m_{H_2} is the mass of the molecule. The diffusion flow

and impingement rate for oxygen are obtained analogously.

Self-consistent equations for the hydrogen and oxygen concentrations near the surface (i.e., for $n^s_{H_2}$ and $n^s_{O_2}$) are obtained by the mass conservation requirement. Recalling Eq. (5), we obtain

$$2S_{O_2}(\Theta)F_{O_2} = f_{H_2} \tag{11a}$$

and

$$S_{O_2}(\Theta)F_{O_2} = f_{O_2}. \tag{11b}$$

Thus, at a given temperature, we have three independent variables (Θ, $n^s_{H_2}$, and $n^s_{O_2}$). In the hydrogen excess regime, these variables are given by Eqs. (3) and (11), and at oxygen excess, by Eqs. (4) and (11).

Finally, we need to describe the heat-transfer process since the energy balance is vital for the ignition process. In the present case we should consider two power generating terms (the external resistive heating, Q_e, and the chemical power, Q_c) and one power loss term (Q_l), due to heat losses to the gas (power losses due to radiation and heat conduction via the wire connections are negligible). Thus, we have the following equation for the catalyst temperature

$$C\frac{dT_s}{dt} = Q_c + Q_e - Q_l, \tag{12}$$

where $C = \pi r_s^2 \rho c_p$ is the heat capacity per unit length of the wire and c_p and ρ are the heat capacity per gram and the density of platinum, respectively.

The heat flow (per unit length of the platinum wire) from the catalyst to the gas phase, may be written as

$$Q_l = h(T_s - T_0), \tag{13}$$

where $h = 2\pi\lambda/\ln(R_{hl}/r_s)$, and λ is the thermal conductivity of the gas mixture. (Calibration runs with only resistive heating verified that this approximation of the heat loss is appropriate.) In addition, we have

$$Q_c = N\Delta H r^f_{H_2O} \tag{14}$$

and

$$Q_e = \begin{cases} \beta h t & \text{at } t < t_{ign} \\ \beta h t_{ign} & \text{at } t > t_{ign}, \end{cases} \tag{15}$$

where $N = 2\pi r_s/\sigma$ is the number of catalytically active sites (per unit length of the wire, $r^f_{H_2O}$ the reaction rate defined by Eq. (5), $\Delta H = 4 \times 10^{-19}$ J the reaction exothermicity per produced H_2O molecule, t_{ign} the time of ignition, and β the heating rate (in degrees Kelvin per second). Note that Eq. (15) at $t < t_{ign}$ corresponds to a linear increase in the catalyst temperature if $Q_c = 0$. The approximation of a linear heating rate, compared to the successive stepwise increase in the experiment, is good as long as the value of β is adjusted to mimic the time averaged heating rate in the experiment. The equations derived above make it possible to self-consistently describe ignition in the system under consideration.

5. THEORETICAL RESULTS

5.1. *Qualitative Analysis and Derivation of Analytical Expressions for* T_{ign}

The traditional theory of ignition is based on analysis of stability of the energy balance and flow in the SS approximation (*1*). In particular, the ignition temperature is defined by

$$\frac{dQ_c}{dT} = h. \tag{16}$$

Employing this equation with some reasonable simplifications, we can obtain a simple analytical expression for the ignition temperature. This expression may be used as a guide in the discussion of the results of numerical simulations presented in Section 5.2.

As a first approximation, we neglect the mass transport limitations at $T \le T_{ign}$. Second, we assume that before and during ignition the surface is almost completely covered by hydrogen. The latter assumption is definitely correct at $\alpha > \alpha^0_{cr}$ (in this case, according to our calculations, ignition occurs at $\Theta_H \approx 0.95$). In fact, the surface can be almost completely covered by hydrogen

even for $\alpha_{cr}^{l} < \alpha < \alpha_{cr}^{0}$ (see Fig. 4). In our analysis of the interval $\alpha_{cr}^{l} < \alpha < \alpha_{cr}^{0}$, we start from this solution.

Due to the large coverage combined with the stronger coverage dependence of the oxygen sticking coefficient compared to hydrogen, we can neglect the first term in Eq. (3) and rewrite it as

$$(1 - \Theta)^{y} \approx k_{H_2}^{d}(1)/(S_{H_2}(0)F_{H_2}), \quad (17)$$

where $k_{H_2}^{d}(1) = \nu \exp(-E_d^l/T)$ is the desorption rate near saturation, i.e., at $\Theta \approx 1$, and E_d^l is the corresponding activation energy for desorption. (This means that the hydrogen adsorption and desorption rates are much larger than the oxygen adsorption rate, which is always fulfilled at sufficiently large Θ). Then, employing Eqs. (5), (14), and (17), we obtain

$$Q_c = 2N\Delta H S_{O_2}(0)F_{O_2} \left(\frac{\nu}{S_{H_2}(0)F_{H_2}}\right)^{x/y} \exp[-xE_d^l/yT]. \quad (18)$$

Substituting this expression into Eq. (16) and neglecting only the temperature dependencies of the impingement rates F_{H_2} and F_{O_2}, we derive

$$T_{ign} = (xE_d^l/y)/\ln\left\{\frac{2xN\Delta H S_{O_2}(0)F_{O_2}E_d^l}{yT_{ign}^2 h}\left(\frac{\nu}{S_{H_2}(0)F_{H_2}}\right)^{x/y}\right\}. \quad (19)$$

Using realistic values of various parameters, one can easily verify that the absolute value of the right-hand factor in the brackets $\{\cdots\}$ is several orders of magnitude larger than the left-hand factor. Omitting the latter factor, we obtain the following very simple approximate expression for the ignition temperature

$$T_{ign} \approx E_d^l/\ln\left(\frac{\nu}{S_{H_2}(0)F_{H_2}}\right). \quad (20)$$

According to Eq. (20), the ignition temperature depends primarily on the rate constants for hydrogen desorption and adsorption. The effect of other parameters on the ignition temperature is minor. A sensitivity analysis of these parameters, by employing Eq. (19) or numerical calculations, shows that the latter conclusion is valid (see below). Qualitatively, Eq. (20) already offers an explanation for the experimentally observed rise in T_{ign} with increasing hydrogen partial pressure (Fig. 7), since an increase of the latter reduces the value of the denominator in Eq. (20).

TABLE I

Values of Various Parameters Employed in Calculations

Parameter	Value	Dimension
$S_{O_2}(0)$	0.02	Dimensionless
$S_{H_2}(0)$	0.05	Dimensionless
ν	10^{13}	s^{-1}
D_{H_2}	0.63	cm^2/s
D_{O_2}	0.18	cm^2/s
R_{H_2}	1.6	cm
R_{O_2}	0.4	cm
R_{ht}	0.4	cm
σ	4	$Å^2$
r_s	0.063	mm
ΔH	4×10^{-19}	J
β	0.1	K/s
$p_{H_2} + p_{O_2}$	45	Torr
p_{tot}	760	Torr
λ	0.024	W/m · K

5.2. *Numerical Calculations*

Using the equations derived in Section 4 and the parameters presented in Table 1, we can now explore the ignition kinetics and condition in more detail. Typical kinetic curves are shown in Fig. 5. Figure 5a shows five calculated T vs t curves for different α. The results clearly show a trend of increasing T_{ign} with increasing α, as in the experiment. Figure 5b shows the associated surface coverages, which drop after T_{ign}. Figures 5c and 5d show the time evolution of the H_2 and O_2 concentrations just outside the surface, normalized to the correspond-

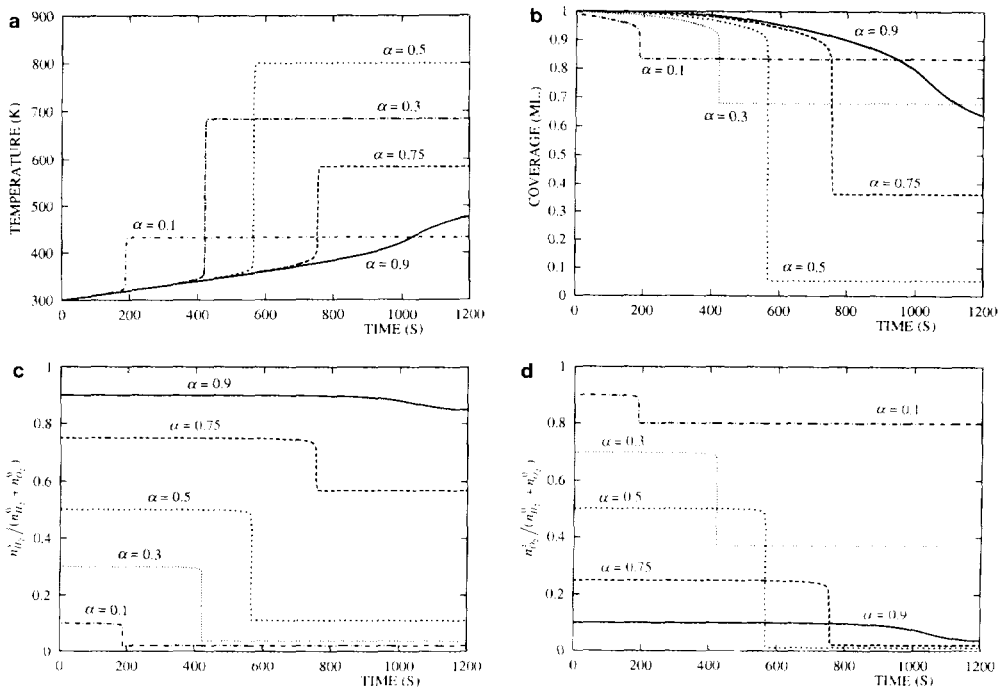

FIG. 5. Catalyst temperature (a) and total coverage (b) and hydrogen (c) and oxygen (d) concentrations near the surface as functions of time for $p_{H_2} + p_{O_2} = 45$ Torr $= 0.059\, p_{tot}$ ($p_{tot} = 760$ Torr is the total pressure of the gas mixture) at $\alpha = 0.1$, 0.3, 0.5, 0.75, and 0.9 (note that the ignition temperature increases with increasing α as in the experiment (Figs. 2 and 7). The results were obtained with $x = 3$, $y = 0.5$, $z = 1$, $A = 7$ kcal/mol, and $\beta = 0.1$ K/s.

ing concentrations in the unperturbed gas mixture.

In all cases, the reaction is governed by surface kinetics and only marginally affected by mass transport before and at ignition. However, after ignition the reaction becomes diffusion limited as illustrated in Figs. 5c and 5d. In this regime, the global reaction rate is maximized when the diffusion flow of hydrogen is equal to twice that of oxygen [cf. Eqs. (9)–(11)]. In this case the reactant concentrations close to the surface will be very low, i.e., when

$$D_{H_2} n^0_{H_2} / \ln(R_{H_2}/r_s) \approx 2 D_{O_2} n^0_{O_2} / \ln(R_{O_2}/r_s).$$

From this condition, we obtain $n^0_{H_2}/n^0_{O_2} = 0.76$, and accordingly $\alpha_{opt} = 0.43$ (subscript opt for optimal). At $\alpha \approx \alpha_{opt}$, the surface coverage is very small after ignition and the reaction rate is maximized. This is why the surface coverage after ignition in Fig. 5b is lowest for $\alpha = 0.5$, which is close to α_{opt}. If $\alpha < \alpha_{opt}$ (e.g., $\alpha = 0.1$ in Fig. 5), the reaction after ignition is limited by hydrogen diffusion. In this case the surface, which is covered by hydrogen prior to ignition (if not $\alpha < \alpha^{I}_{cr}$), becomes covered by oxygen after ignition. Note, however, that the discontinuous change in reactant coverage occurs shortly *after* ignition. Thus, this change in coverage is a consequence, not a reason for ignition. The reason for ignition is the decrease in the hydrogen coverage due to an increasing desorption rate with increasing temperature. If $\alpha > \alpha_{opt}$ (e.g., $\alpha = 0.75$ in Fig. 5), the reaction after ignition is limited by oxygen diffusion. In this case, the surface coverage is dominated by hydrogen both before and after ignition.

Comparing the calculated kinetic curves

(Fig. 5a) with that obtained in the experiment (Fig. 2), two comments are called for. First, the SS theory does not reproduce the overshoot in the temperature vs time curve just after ignition. This overshoot, as we have already pointed out in Section 3, is attributed to the larger concentration of reactants available at the moment of ignition compared to later times, when there is a depletion of reactants close to the catalyst; i.e., the overshoot is connected with the non-steady-state mass transport just after ignition. The latter effect is of course not described in the SS approximation. Second, the theory overestimates the catalyst temperature after ignition. This is connected with a difference between the experimental situation and the model, concerning mass transport, when the reaction rate is high and the gradients are strong. Prior to ignition the reaction rate is low and the boundary condition for hydrogen diffusion with a characteristic radius of $R_{H_2} \approx 1.6$ cm (Section 4.2) is a good approximation. However, in the SS state after ignition, the reaction rate is high and the gas flow is vital for sustaining the reaction. In this case, since the gas-flow velocity is small and R_{H_2} is larger than the cell radius, there will be in the experiment a strong deviation from the cylindrical symmetry assumed in the model, which consequently overestimates the transport of reactants to the catalyst and thus leads to an overestimation of the chemical power. The latter can be taken into account in more detailed simulations (such calculations are in progress). Both of these effects are important after ignition but negligible at and before ignition.

We now turn to the central point, namely the variation of T_{ign} with α (Figs. 6 and 7). Both the calculated and measured ignition temperatures increase with increasing α, i.e., with the increase in relative hydrogen pressure (*41*). The model offers a simple explanation for this behavior. As α increases, the hydrogen impingement rate and thus the hydrogen coverage increases, while the oxygen impingement rate decreases. At a given temperature the rate of reaction, and thus the chemical heating, therefore decreases with increasing α. Consequently the temperature must be increased as α increases, in order to create more unoccupied sites (via hydrogen desorption) before the ignition condition is reached.

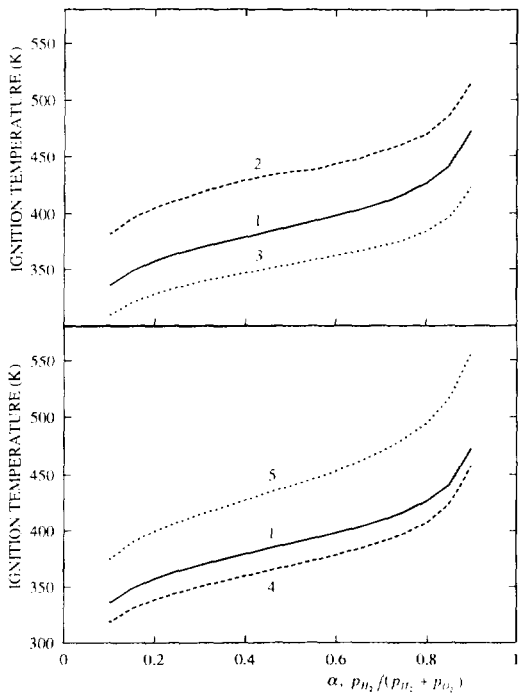

FIG. 6. Ignition temperature as a function of α, illustrating the sensitivity of the parameters x, y, z, and A. Curve 1 represents the basic parameter set with $x = 3$, $y = 0.5$, $z = 1$, and $A = 7$ kcal/mol. In curves 2–5, one parameter has been given another value. Curve 2, $A = 5$ kcal/mol; 3, $x = 2$; 4, $y = 1$; and 5, $z = 3$.

In Fig. 6, T_{ign} vs α is shown for various values of the parameters A, x, y, and z. In all cases, the experimentally observed trend is qualitatively reproduced, but the parameter values influence the quantitative agreement. A decrease in A is equivalent to an increase in the activation energy for hydrogen desorption near saturation coverage [see Eq. (8)] and consequently results in an increase in T_{ign} (see Eq. (20) and cf. curves 1 and 2 corresponding to $A = 7$ and 5 kcal/mol, respectively). A decrease of x

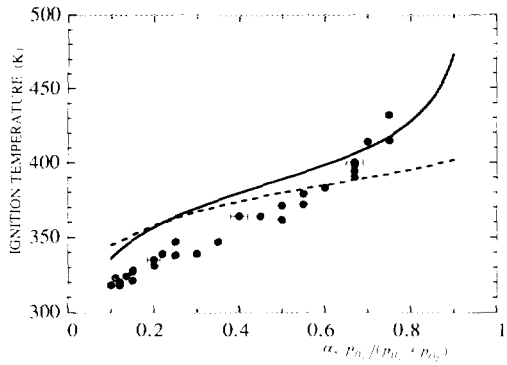

FIG. 7. Ignition temperature as a function of α. (●) Experimental data. (—) Simulation with $x = 3$, $y = 0.5$, $z = 1$, and $A = 7$ kcal/mol. (---) Equation (19) with $x = 3$, $y = 0.5$, and $E_d^1 = 13$ kcal/mol. The theoretical and experimental data have been obtained at $p_{H_2} + p_{O_2} = 45$ Torr.

(the exponent for the coverage dependence of the oxygen sticking coefficient) facilitates oxygen adsorption. Then the reaction rate inreases at a given temperature, and T_{ign} decreases (cf. curves 1 and 3 corresponding to $x = 3$ and 2, respectively). An increase of y (the exponent for the coverage dependence of the hydrogen sticking coefficient) suppresses hydrogen adsorption and the number of empty sites becomes higher, the reaction rate increases, and T_{ign} will consequently decrease (cf. curves 1 and 4 corresponding to $y = 0.5$ and 1, respectively). Finally, an increase of z (the exponent in the coverage dependence of the activation energy for hydrogen desorption) results in a weaker coverage dependence for hydrogen desorption (but a steeper slope near saturation), which leads to an increase in T_{ign} (cf. curves 1 and 5 corresponding to $z = 1$ and 3, respectively). The α dependence of T_{ign} is fairly insensitive to reasonable variations of the parameters A, x, y, and z (the α dependence, i.e., the slope of T_{ign} vs α, becomes a little stronger with decreasing y and/or increasing x and/or increasing z).

In Fig. 7, the experimentally measured T_{ign} vs α (solid circles) are compared with the full numerical solution (full curve), using what we consider to be the best set of parameter values, $x = 3$, $y = 0.5$, $z = 1$, and $A = 7$ kcal/mol. As discussed in Section 4.1, these values are based on existing literature data. The agreement with the experiment is in our opinion good. For comparison we have included also in Fig. 7 the results from the analytical solution, Eq. (19) (dashed curve), using the same parameters as in the numerical solution, but with a constant value of $E_d^1 = 13$ kcal/mol (*42*). This approximation also gives a reasonable agreement but deviates from the experiment and numerical solution at large α. This is due to the constant value of E_d^1 employed, which is representative for $\alpha \approx 0.1$–0.4. With increasing α, the oxygen impingement rate becomes lower, and therefore a successively lower hydrogen coverage is required to reach ignition (in order to compensate the lowered oxygen impingement rate with a larger oxygen adsorption rate). A lower hydrogen coverage means a larger E_d^1. Inspection of Eq. (19) [or (20)] shows that if this effect is included, it will adjust the analytical solution for T_{ign} to higher values at large α, in closer agreement with the experiment and the full numerical results.

For α-values >0.75, no clear ignition was experimentally observed. The ignition condition, Eq. (16), thus does not seem to be realized for any temperature in that range. Upon increasing the temperature, the system instead moved smoothly from kinetic to mass transport control. Qualitatively, this indicates that the slope of $Q_c(T)$ vs T never exceeds h [Eq. (16)]. As discussed above, this can be connected with the increasing hydrogen poisoning for high α-values. The model also predicts the absence of ignition, but only at $\alpha \geq 0.9$ (see, e.g., Fig. 5a with $\alpha = 0.9$, where ignition is absent).

We have thus obtained a good agreement between theory and experiment for T_{ign} vs α and a clear understanding of why and how T_{ign} increases with α. The main reason is the weaker coverage dependence for hydrogen adsorption compared to that of oxygen adsorption. Furthermore the slope of the T_{ign} vs α-curve is affected by the experimentally demonstrated (*28*) coverage dependence of the activation energy for H_2 desorption.

6. SUMMARY AND CONCLUSION

We have developed a model for simulation of ignition on catalytic wires and compared its predictions with experimental results. The approach, based on the steady-state approximation, explicitly takes into account the reaction kinetics, mass and heat transport processes, and finite velocity of the carrier-gas flow.

Employing the derived general equations, we have studied the effect of various kinetic parameters on the ignition temperature in the hydrogen–oxygen reaction on a Pt wire. The main reason for ignition is a decrease in surface coverage of hydrogen, with increasing temperature, due to desorption, which in turn creates new sites for reaction and an increasing reaction rate. Shortly after ignition, a stepwise change in the reactant coverages, toward an oxygen-covered surface, takes place if the relative hydrogen pressure is not too high.

With reasonable values of various kinetic parameters, the experimentally observed trend of increasing ignition temperature with increasing relative hydrogen pressure is reproduced, but the trend is somewhat weaker in the model than in the experiment.

We have also identified an interesting regime for further studies, where two solutions exist in coverage and reaction rate.

ACKNOWLEDGMENTS

Financial support from NUTEK (Contract 91-56678p), the National Swedish Board for Technical Development (Contract 83-05405p), and the Swedish Research Council for Engineering Sciences (Contract 92-951) is gratefully acknowledged. One of us (V. P. Zhdanov) is thankful to the Royal Swedish Academy of Science, the Swedish Institute, and the NFR for supporting his visits to Chalmers University of Technology.

REFERENCES

1. Frank-Kamenetskii, D. A., "Diffusion and Heat Transfer in Chemical Kinetics," 2nd ed. Plenum, New York, 1969.
2. Schwartz, A., Holbrook, L. L., and Wise, H., *J. Catal.* **21,** 199 (1971).
3. Cordoso, M. A. A., and Luss, D., *Chem. Eng. Sci.* **24,** 1699 (1969).
4. Rader, C. G., and Weller, S. W., *AIChE J.* **20,** 515 (1974).
5. Sheintuch, M., and Schmidt, J., *Chem. Eng. Commun.* **44,** 33 (1986); Sheintuch, M., *Chem. Eng. Sci.* **44,** 1081 (1989).
6. Cho, P., and Law, C. K., *Comb. Flame* **66,** 159 (1986).
7. (a) Russberg, G. N., Thesis, Chalmers University of Technology, Göteborg, 1989; (b) Fassihi, M., M.Sc. thesis, University of Gothenburg, Göteborg, 1991.
8. Harold, M. P., and Garske, M. E., *J. Catal.* **127,** 524 (1991).
9. Harold, M. P., and Garske, M. E., *J. Catal.* **127,** 553 (1991).
10. Garske, M. E., and Harold, M. P., *Chem. Eng. Sci.* **47,** 623 (1992).
11. Kasemo, B., Keck, K.-E., and Högberg, T., *J. Catal.* **66,** 441 (1980).
12. Keck, K.-E., Kasemo, B., and Högberg, T., *Surf. Sci.* **126,** 469 (1983).
13. Keck, K.-E., and Kasemo, B., *Surf. Sci.* **167,** 313 (1986).
14. Christmann, K., Ertl, G., and Pignet, T., *Surf. Sci.* **54,** 365 (1976).
15. Norton, P. R., Davies, J. A., and Jackman, T. E., *Surf. Sci.* **121,** 103 (1982).
16. Hellsing, B., Kasemo, B., and Zhdanov, V. P., *J. Catal.* **132,** 210 (1991).
17. Ljungström, S., Kasemo, B., Rosén, A., Wahnström, T., and Fridell, E., *Surf. Sci.* **216,** 63 (1989).
18. Lundgren, S., Keck, K.-E., and Kasemo, B., submitted for publication.
19. Norton, P. R., *in* "The Chemical Physics of Solid Surfaces and Heterogeneous Catalysis" (D. A. King and D. P. Woodruff, Eds.), Vol. 4, p. 70. Elsevier, Amsterdam, 1982.
20. Verheij, L. K., Hugenschmidt, M. B., Anton, A. B., Poelsema, B., and Comsa, G., *Surf. Sci.* **210,** 1 (1989).
21. Verheij, L. K., Hugenschmidt, M. B., Poelsema, B., and Comsa, G., *Surf. Sci.* **233,** 209 (1990).
22. Ogle, K. M., and White, J. M., *Surf. Sci.* **139,** 43 (1984).
23. Germer, T. A., and Ho, W., *Chem. Phys. Lett.* **163,** 449 (1989).
24. Anton, A. B., and Codogan, D. C., *J. Vac. Sci. Technol. A* **9,** 1890 (1991).
25. Williams, W. R., Marcus, C. M., and Schmidt, L. D., *J. Phys. Chem.* **96,** 5922 (1992).
26. Kwasniewski, V. J., and Schmidt, L. D., *J. Phys. Chem.* **96,** 5931 (1992).
27. Fisher, G. B., Gland, J. L., and Schmieg, S. J., *J. Vac. Sci. Technol.* **20,** 518 (1982).
28. Zhdanov, V. P., *Surf. Sci.* **169,** 1 (1986).
29. Gland, J. L., Fisher, G. B., and Kollin, E. B., *J. Catal.* **77,** 263 (1982).

30. Kasemo, B., and Törnqvist, E., *Phys. Rev. Lett.* **44,** 1555 (1980).
31. Campbell, C. T., Ertl, G., Kuipers, H., and Segner, J., *Surf. Sci.* **107,** 220 (1981).
32. Luntz, A. C., Williams, M. D., and Bethune, D. S., *J. Chem. Phys.* **89,** 4381 (1988).
33. Salmerón, M., Gale, R. J., and Somorjai, G. A., *J. Chem. Phys.* **70,** 2807 (1979).
34. Luntz, A. C., Brown, J. K., and Williams, M. D., *J. Chem. Phys.* **93,** 5240 (1990).
35. Ertl, G., *in* "Advances in Catalysis" (D. D. Eley, H. Pines, and P. B. Weisz, Eds.), Vol. 37, p. 213. Academic Press, New York, 1990; Schüth, F., Henry, B. E., and Schmidt, L. D., *in* "Advances in Catalysis" (D. D. Eley, H. Pines, and P. B. Weise, Eds.) Vol. 39, p. 57. Academic Press, New York, 1993.
36. Yablonskii, G., Bykov, V., Gorban, A., and Elokhin, V., "Kinetic Models of Catalytic Reactions," Comprehensive Chemical Kinetics, Vol. 32. Elsevier, Amsterdam, 1991.
37. Mikhailov, A. S., "Foundations of Synergetics I." Springer, Berlin, 1990.
38. Bar, M., Zülicke, Ch., Eiswirth, M., and Ertl, G., *J. Chem. Phys.* **96,** 8595 (1992).
39. Evans, J. W., *J. Chem. Phys.* **97,** 572 (1992).
40. Zhdanov, V. P., submitted for publication.
41. This is also confirmed by a study of Cho and Law (6), who measured ignition temperatures for H_2–O_2 mixtures over a Pt wire in the range $0.05 < \alpha < 0.24$. The slope of their T_{ign} vs α curve were in good agreement with the present results, but their ignition temperatures were slightly higher.
42. This value was obtained as follows. Numerical integration of Eq. (12) and utilization of the rest of the coupled equations in Section 4 (and with boundary conditions) in conjunction with the ignition criterion, Eq. (16), yields the coverage at ignition, $\Theta_{ign} \approx 0.95$, for $\alpha \approx 0.1$–0.4. With the chosen parameter set of z and A, the activation energy at this coverage [Eq. (8)] is obtained: $E_d^1 \approx 13$ kcal/mol.